

Article

Assessment of MERRA-2 Surface PM_{2.5} over the Yangtze River Basin: Ground-based Verification, Spatiotemporal Distribution and Meteorological Dependence

Lijie He ¹ , Aiwen Lin ^{1,*}, Xinxin Chen ², Hao Zhou ³ , Zhigao Zhou ¹ and Peipei He ⁴

¹ School of Resource and Environmental Science, Wuhan University, Wuhan 430079, China; 13035128257@163.com (L.H.); leelong@whu.edu.cn (Z.Z.)

² Hubei Key Laboratory of Critical Zone Evolution, School of Earth Sciences, China University of Geosciences, Wuhan 430074, China; 18270921625@163.com

³ MOE Key Laboratory of Fundamental Physical Quantities Measurement, School of Physics, Huazhong University of Science and Technology, Wuhan 430074, China; zhouh@hust.edu.cn

⁴ College of Surveying and Geo-Informatics, North China University of Water Resources and Electric Power, Zhengzhou 450045, China; hepei@ncwu.edu.cn

* Correspondence: awlin@whu.edu.cn; Tel.: +86-137-0719-1591

Received: 8 January 2019; Accepted: 20 February 2019; Published: 23 February 2019



Abstract: A good understanding of how meteorological conditions exacerbate or mitigate air pollution is critical for developing robust emission reduction policies. Thus, based on a multiple linear regression (MLR) model in this study, the quantified impacts of six meteorological variables on PM_{2.5} (i.e., particle matter with diameter of 2.5 μm or less) and its major components were estimated over the Yangtze River Basin (YRB). The 38-year (1980–2017) daily PM_{2.5} and meteorological data were derived from the newly-released Modern-Era Retrospective Analysis and Research and Application, version 2 (MERRA-2) products. The MERRA-2 PM_{2.5} was underestimated compared with ground measurements, partly due to the bias in the MERRA-2 Aerosol Optical Depth (AOD) assimilation. An over-increasing trend in each PM_{2.5} component occurred for the whole study period; however, this has been curbed since 2007. The MLR model suggested that meteorological variability could explain up to 67% of the PM_{2.5} changes. PM_{2.5} was robustly anti-correlated with surface wind speed, precipitation and boundary layer height (BLH), but was positively correlated with temperature throughout the YRB. The relationship of relative humidity (RH) and total cloud cover with PM_{2.5} showed regional dependencies, with negative correlation in the Yangtze River Delta (YRD) and positive correlation in the other areas. In particular, PM_{2.5} was most sensitive to surface wind speed, and the sensitivity was approximately $-2.42 \mu\text{g m}^{-3} \text{m}^{-1} \text{s}$. This study highlighted the impact of meteorological conditions on PM_{2.5} growth, although it was much smaller than the anthropogenic emissions impact.

Keywords: MERRA-2; PM_{2.5}; meteorological variables; Yangtze River basin

1. Introduction

Since its reform and opening up (1978 onward), with the rapid development of urbanization and industrialization, China has become one of the most polluted areas [1–6]. PM_{2.5} (i.e., particle matter with diameter of 2.5 μm or less) is an important metric for air pollution, which has attracted considerable attention. When these particles are breathed in, they can lead to premature deaths [7–10]. In addition, they can effectively scatter and absorb solar radiation, thereby reducing atmospheric visibility and producing significant climate impacts [11–19].

A large number of studies have been performed to analyze potential causes of recent heavy air pollution in China and its effective solutions. Most of them have suggested that the excessive increase in anthropogenic emissions was the most important reason for PM_{2.5} growth in China [20–25]. For example, Guo et al. [21] found that during Asia-Pacific Economic Cooperation (APEC) China 2014, the air quality in Beijing was effectively improved mainly due to the emission control measures. Furthermore, Ren et al. [22] confirmed that Beijing's air pollution during the 2015 China Victory Day Parade mainly came from traffic and cooking emissions. Additionally, Larkin [23] reported that rapid urban sprawl led to a significant growth in NO₂ and PM_{2.5} air pollution at 830 cities in East Asia from 2000 to 2010. All of these previous studies indicated that anthropogenic emissions were main sources of PM_{2.5} growth in China.

However, air pollution was observed to have seasonal and interannual variations, although anthropogenic emissions were continuously increasing. Obviously, these variations were caused by local meteorological changes [3,26–34]. Empirical Studies on the sensitivities of PM_{2.5} concentrations to meteorological conditions were exhibited in Table 1. Tai et al. [26] revealed that based on a multiple linear regression (MLR) model, local meteorological factors could explain up to 50% of daily PM_{2.5} variability in the USA from 1998 to 2008. Westervelt et al. [27] further emphasized the maximum impact of temperature, wind speed and precipitation on PM_{2.5} concentrations at global scale. Additionally, Harrison et al. [28] revealed that PM_{2.5} concentrations were more strongly correlated with easterly winds from the European mainland than with the local traffic sources. Similarly, in three European cities (Athens, London and Madrid), local meteorological conditions also had significant impacts on particulate matters (PM_{2.5} and PM₁₀) [29]. In Saudi Arabia, both PM₁₀ and PM_{2.5} were negatively related to relative humidity; however, they were positively correlated with wind speed and temperature [30]. Recently, He et al [3] discovered that meteorological conditions were the primary factors of daily variations in five major air pollutants (PM_{2.5}, O₃, NO₂, SO₂ and CO) during 2014–2015 in China. Wang et al. [31] further confirmed that an air stagnation event, characterized by weak wind speed, no precipitation and high temperature, easily led to haze in China. Furthermore, in the Beijing urban area, wind rose plots showed that low wind speeds of northeastern or southwestern winds usually led to high black carbon (BC) concentrations [32]. In 68 major cities of China, Yang et al. [33] reported that ground PM_{2.5} concentrations were associated with local meteorological conditions at seasonal, yearly and regional scales. The impacts of PM_{2.5} pollution on atmospheric visibility, occupational health and occupants' behaviors were also estimated in China [34].

Even though extensive research has been carried out to explore the relationship between meteorological conditions and air pollution, most of it has focused on the impact in daily PM_{2.5} variability for a short term, such as during a haze event. However, studies on the sensitivity of air pollution to long-term meteorological changes are still limited, mainly due to a lack of data [35,36]. The newly-released Modern-Era Retrospective Analysis and Research and Application, version 2 (MERRA-2) product could provide daily PM_{2.5} and meteorological data after 1980 for free, giving us an opportunity to quantify the long-term effect of meteorological conditions on PM_{2.5} [37–40]. An important advancement of the MERRA-2 aerosol reanalysis product was that it not only assimilated the bias-corrected 550nm-AODs from the space-based AVHRR (Advanced Very High-Resolution Radiometer) and MODIS (Moderate Resolution Imaging Spectroradiometer) instruments, but also assimilated the non-bias-corrected 550nm-AODs from the space-based MISR (Multiangle Imaging Spectroradiometer) and the ground-based AERONET (Aerosol Robotic Network) stations. Furthermore, five types of aerosols, including dust, sea salt, sulfate (SO₄), black carbon (BC) and organic carbon (OC), were also simulated based on the NASA Global Modeling and Assimilation Office (GMAO) Earth system model (GEOS-5) and the Goddard Chemistry, Aerosol, Radiation and Transport (GOCART) aerosol module. Notably, the MERRA-2 AOD assimilation in GEOS-5 involved very careful cloud screening and homogenization of the observing system through neural net scheme, thus providing high-quality AOD observations [37,38]. In general, the newly-released MERRA-2 atmospheric reanalysis was widely used for studying global climate change and regional environment due to its high data quality, continuous spatial and temporal resolutions and diverse aerosol species.

The Yangtze River Basin (YRB) was divided into four regions due to their diverse underlying surfaces and aerosol sources, from east to west, followed by the Yangtze River Delta (YRD), Central China (CC), Sichuan Basin (SB) and the source of the YRB (SYR) (Figure 1) [8,9,21]. Both YRD and CC had an average elevation of no more than 50m and had frequent urbanization and industrialization activities, resulting in high aerosol loadings [8,9]. However, the YRD might be similarly affected by sea salt aerosols. In the SB, the unique basin topography would lead to a low wind speed, high relative humidity and cloudy meteorological condition, which was different from its surrounding areas. It was not conducive to the diffusion and dilution of aerosol particles [8]. By contrast, most of the SYR were located in the Qinghai-Tibet Plateau, which had unique plateau weather and little anthropogenic activities. Coarse particles were the major aerosol type; for example, occasional large areas of sand and dust were transported here via surface winds in spring [31]. Overall, such diverse underlying surfaces, aerosol sources and meteorological conditions were conducive to studying the sensitivities of different PM_{2.5} components to local meteorological conditions. Therefore, the YRB was selected as the region of interest in this study.

This study aimed to (1) verify the performance of MERRA-2 PM_{2.5} reanalysis; (2) make a good knowledge of spatiotemporal distributions of each PM_{2.5} component over the YRB from 1980 to 2017; and (3) reveal the quantified impacts of major meteorological factors (including surface wind speed, surface temperature, precipitation, relative humidity, total cloud cover and boundary layer height) on each PM_{2.5} component. The structure was organized as follows. Section 2 introduced data and analytical methods. Section 3 analyzed MERRA-2 PM_{2.5} verification and spatiotemporal distributions. The sensitivities of different PM_{2.5} components to meteorological variables were further discussed in Section 4. Finally, conclusions were provided in Section 5.

Table 1. Empirical Studies of the impacts of meteorological conditions on PM_{2.5} (i.e., particle matter with diameter of 2.5 µm or less) concentrations.

Study Areas	Methods	Meteorological Variables	Pollution Indicators	Main Conclusions
United states (1998–2008) [26]	Multiple linear regression (MLR)	Surface temperature, precipitation, total cloud cover, wind speed, wind direction and relative humidity	PM _{2.5} , SO ₄ , OC, EC *	Daily meteorological variables could explain up to 50% changes of PM _{2.5} in the USA.
Global scale (2005–2016) [27]	Chemistry-climate model	Surface temperature, precipitation, total cloud cover, wind speed, relative humidity and pressure	PM _{2.5}	PM _{2.5} concentrations were most sensitive to surface temperature, wind speed and precipitation.
United Kingdom (2009) [28]	Regression analyses	Wind speed and direction	PM ₁₀ , PM _{2.5} , NO _x *	PM _{2.5} concentrations exhibited a stronger correlation with easterly winds from the European mainland than with the local traffic sources.
Three European cities (2005–2015) [29]	Principal component and regression analyses	Wind velocity, temperature, relative humidity, precipitation, solar radiation and atmospheric pressure	PM ₁₀ , PM _{2.5}	Local meteorological conditions had a significant impact on air pollutions.

Table 1. Cont.

Study Areas	Methods	Meteorological Variables	Pollution Indicators	Main Conclusions
Europe, US, China (2013–2016) [30]	MLR	Air stagnation event (i.e., daily 10-m wind speed $< 3.2 \text{ m s}^{-1}$, 500-hPa tropospheric wind speed $< 13 \text{ m s}^{-1}$ and no precipitation)	PM _{2.5}	Compared to no-stagnation conditions, air stagnation events in winter could increase PM _{2.5} concentrations in the United States, Europe and China by 46%, 68% and 60%, respectively.
Saudi Arabia (2014–2015) [31]	MLR	Relative humidity, wind speed and temperature	PM _{2.5} , PM ₁₀	Both PM ₁₀ and PM _{2.5} were anti-correlated with relative humidity, but positively related to wind speed and temperature.
Beijing China (2005–2013) [32]	MLR	Relative humidity and wind speed	Black carbon (BC)	High BC concentrations were usually related to poor visibility and low wind speed.
China (2013–2014) [33]	Multivariate analysis	Relative humidity, wind speed, surface pressure and temperature	PM _{2.5}	PM _{2.5} was significantly correlated with meteorological conditions in China.

* SO₄, OC, EC, NO_x refer to sulfate, organic carbon, element carbon and nitrogen oxides, respectively.

2. Data and Methods

2.1. Data

The MERRA-2 atmospheric reanalysis product was newly released by the NASA Global Modeling and Assimilation Office (GMAO) in 2017. Based on the NASA GMAO Earth system model version 5 (GEOS 5) and the Goddard Chemistry, Aerosol, Radiation and Transport (GOCART) aerosol module, the gridded aerosol data of MERRA-2 were assimilated with satellite and ground observations. More details on MERRA-2 PM_{2.5} treatment could be found in [37–40], and were briefly described here. MERRA-2 PM_{2.5} concentrations were calculated by Equation (1):

$$\text{PM}_{2.5} = 1.375 \times \text{SO}_4 + 1.6 \times \text{OC} + \text{BC} + \text{Dust}_{2.5} + \text{SS}_{2.5} \quad (1)$$

Here, SO₄, OC, BC, Dust_{2.5} and SS_{2.5} represented sulfate, organic carbon, black carbon, dust and sea-salt particulate matter with a diameter of less than 2.5 μm from the GOCART aerosol module, respectively. Notably, the nitrate particulate matter primarily emitted by vehicle exhaust and industrial production was lacking in the MERRA-2 PM_{2.5} reanalysis, probably leading to biases when compared with ground measurements. In order to verify the performance of the MERRA-2 PM_{2.5} product, we compared MERRA-2 PM_{2.5} with two-year (2015–2016) daily mean PM_{2.5} ground observations from 476 state-controlled air quality monitoring stations over the YRB (Figure 1). By using the tapered element oscillating microbalance method and/or the beta absorption method, these state-controlled air quality monitoring stations provided hourly and 24-hour average concentrations of six major air pollutants (including PM_{2.5}, PM₁₀, SO₂, NO₂, O₃ and CO) after 2013 [40]. The systematic uncertainty

of ground $PM_{2.5}$ from these air quality monitoring stations was controlled within 15% in accordance with the latest version of China's environmental protection standards [40].

In addition, the spatial and temporal distributions of MERRA-2 $PM_{2.5}$ were further compared with another $PM_{2.5}$ reanalysis product released by the Atmospheric Composition Analysis Group of NASA. Similarly, based on the GEOS-Chem chemical transport model, the satellite-retrieved $PM_{2.5}$ concentrations ($0.01^\circ \times 0.01^\circ$) were estimated by combining column integrated AODs from MODIS (Moderate Resolution Imaging Spectroradiometer), MISR (Multiangle Imaging Spectroradiometer) and SeaWiFS (Sea-Viewing Wide Field of View Sensor) instruments [41,42]. Then, in order to adjust the residual bias, the satellite-derived $PM_{2.5}$ concentrations were calibrated by ground-based observations using a geographically weighted regression (GWR). Hereafter, the $PM_{2.5}$ reanalysis product was abbreviated as GWR $PM_{2.5}$ in this study. As shown in Figure A1, the annual mean GWR $PM_{2.5}$ concentrations were compared with ground $PM_{2.5}$ measurements from 476 state-controlled air quality monitoring stations over the YRB during 2015–2016. A high correlation coefficient ($R = 0.76$) demonstrated a good consistency between GWR $PM_{2.5}$ and ground $PM_{2.5}$, which provided us enough confidence to use the GWR $PM_{2.5}$ product to verify the spatiotemporal distribution of MERRA-2 $PM_{2.5}$.

Since both the non-bias-corrected AODs (MISR and AERONET) and the bias-corrected AODs (MODIS and AVHRR) were assimilated in the MERRA-2 aerosol reanalysis, these above AOD datasets were all not suitable for verifying the MERRA-2 AODs. Therefore, the daily ground AOD observations from five China Aerosol Remote Sensing Network (CARSNET) sites in the YRB during 2013–2016, were selected to be compared with their corresponding MERRA-2 AODs at 550 nm (Figure 1 and Table 2). The CARSNET was a ground aerosol network with approximately 50 sites across China, established by the China meteorological administrations and university research institutes [9,12]. It used Cimel sun photometers to retrieve the Level-1.0 (unscreened) and Level-1.5 (cloud-screened) AOD data at eight wavelengths (340, 380, 440, 500, 675, 870, 1020 and 1640 nm) every 15 minutes [9]. The total uncertainty in the CARSNET AODs was about 0.01 to 0.02 [12]. The CARSNET AODs used in this study were all cloud-screened data. As shown in Figure 1, from east to west, the five CARSNET sites were Lin'an (rural site, 39 m above sea level), Wuhan (urban site, 15 m above sea level), Changde (rural site, 38 m above sea level), Chengdu (urban site, 485 m above sea level) and Shangri-La (remote site, 3280 m above sea level) [12].

The MERRA-2 atmospheric reanalysis product also provided grid-level ($0.05^\circ \times 0.625^\circ$) daily mean meteorological variables data during 1980–2017 (Table 2). They were surface wind speed ($m\ s^{-1}$), surface temperature (K), surface precipitation (mm d⁻¹), relative humidity (%), total cloud cover (%) and boundary layer height (m).

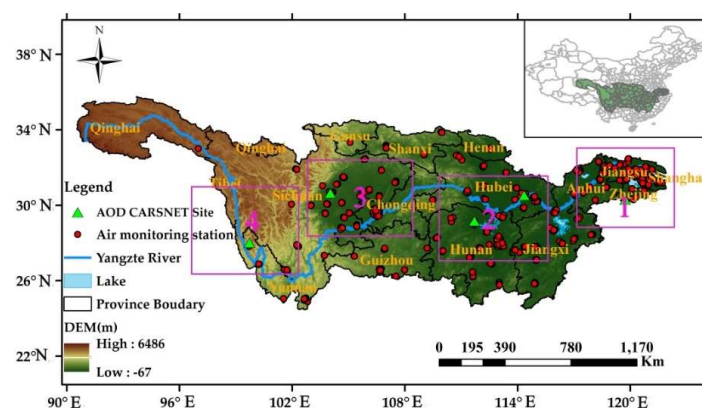


Figure 1. Distribution of ground air monitoring stations and China Aerosol Remote Sensing Network (CARSNET) sites over the Yangtze River Basin (YRB). The YRB was divided into four regions, labeled from 1 to 4, which are the Yangtze River Delta (YRD), Central China (CC), Sichuan Basin (SB) and source of the YRB (SYR).

Table 2. Summary of data used in this study.

		Spatial Resolution	Temporal Coverage	Data Source
PM _{2.5}	MERRA-2 *	0.05° × 0.625°	daily\1980–2017	http://disc.sci.gsfc.nasa.gov/mdisc/
	GWR *	0.01° × 0.01°	daily\1998–2017	http://fizz.phys.dal.ca/~jatmos/martin/?page_id=140
	Ground	\	daily\2015–2016	http://113.108.142.147:20035/emcpublish/
AOD *	MERRA-2	0.05° × 0.625°	daily\2013–2016	http://disc.sci.gsfc.nasa.gov/mdisc/
	CARSNET *	\	daily\2013–2016	\
	Terra, Aqua	0.01° × 0.01°	daily\2016	https://ladsweb.modaps.eosdis.nasa.gov/search/
Meteorological factors	MERRA-2	0.05° × 0.625°	daily\1980–2017	http://disc.sci.gsfc.nasa.gov/mdisc/

* AOD, MERRA-2, GWR, CARSNET refer to Aerosol Optical Depth, Modern-Era Retrospective Analysis and Research and Application, version 2 product, Geographically Weighted Regression product and China Aerosol Remote Sensing Network, respectively.

2.2. Methods

2.2.1. Comparison Analysis

According to [40], grid-level daily mean MERRA-2 PM_{2.5} concentrations were compared with the corresponding ground measurements during 2015–2016 over the YRB by using a series of linear regressions. The regression parameters include slope, y–intercept, correlation coefficient (R), root mean square error (RMSE, Equation (2)), mean absolute error (MAE, Equation (3)) and the relative mean bias (RMB, Equation (4)):

$$RMSE = \sqrt{\frac{1}{n} \sum_{i=1}^n (PM_{2.5(MERRA-2)i} - PM_{2.5(ground)i})^2} \quad (2)$$

$$MAE = \frac{1}{n} \sum_{i=1}^n |PM_{2.5(MERRA-2)i} - PM_{2.5(ground)i}| \quad (3)$$

$$RMB = \left(\overline{PM_{2.5MERRA-2}} / \overline{PM_{2.5ground}} \right) \quad (4)$$

The MERRA-2 PM_{2.5} reanalysis was thought to be reasonably good if RMB ≥ 0.5 [27].

2.2.2. Trend Analysis

Multi-year average trends (1980–2017) in PM_{2.5} and its major components (including SO₄, BC, OC, Dust_{2.5} and SS_{2.5}) were assessed based on a linear regression. Furthermore, their corresponding significant levels were calculated using the Mann-Kendall (MK) nonparametric method. They were described by Equations (5)–(8):

$$S = \sum_{i=1}^{n-1} \sum_{j=n+1}^n \text{sgn}(X_j - X_i) \quad (5)$$

$$\text{sgn}(X_j - X_i) = \begin{cases} +1, & \text{if } (X_j - X_i) > 0 \\ 0, & \text{if } (X_j - X_i) = 0 \\ -1, & \text{if } (X_j - X_i) < 0 \end{cases} \quad (6)$$

$$\text{Var}(s) = \frac{n(n-1)(2n+5) - \sum_{p=1}^q t_p(t_p-1)(2t_p+5)}{18} \quad (7)$$

$$Z = \begin{cases} \frac{S-1}{\sqrt{\text{Var}(S)}}, & \text{if } S > 0 \\ 0, & \text{if } S = 0 \\ \frac{S+1}{\sqrt{\text{Var}(S)}}, & \text{if } S < 0 \end{cases} \quad (8)$$

where S is the statistical value, $\text{Var}(S)$ is the variance of the statistical value S and X_j and X_i represent the annual mean concentrations of the total $\text{PM}_{2.5}$ or its major components in the j th and i th years, respectively. The trend was significant (i.e., p -value < 0.05) only when the standardized test statistics $|Z| > |Z_{(1-\alpha/2)}|$.

2.2.3. Multiple Linear Regression

In order to assess the comprehensive impact of various meteorological factors on $\text{PM}_{2.5}$, the following multiple linear regression (MLR) model was used:

$$y = \beta_0 + \sum_{i=1}^6 \beta_i x_i + \varepsilon_i \quad (9)$$

where the dependent variable y refers to daily mean $\text{PM}_{2.5}$ concentrations (including $\text{PM}_{2.5}$, SO_4 , OC, BC, $\text{Dust}_{2.5}$ and $\text{SS}_{2.5}$) in each $0.05^\circ \times 0.625^\circ$ grid, β_0 is a constant term, x_i is the daily mean meteorological factor described in Section 2.1 and ε_i is the interaction term. Moreover, the slope coefficient β_i can be interpreted as the sensitivity of $\text{PM}_{2.5}$ to changes in one meteorological factor, assuming that the other meteorological variables remain fixed. This was determined via a least-square adjustment [26,27].

3. Results

3.1. Ground-Based Verification of MERRA-2 $\text{PM}_{2.5}$

3.1.1. Regional and Seasonal Comparisons between MERRA-2 and Ground $\text{PM}_{2.5}$

Comparisons of daily mean $\text{PM}_{2.5}$ concentrations derived from MERRA-2 and 476 ground sites over the YRB are presented in Figure 2. The comparison over the YRD (Figure 2b) was superior to other regions of the YRB, with higher R (0.58) and RMB (0.90) values. By contrast, the SB (Figure 2d) produced the worst performance, with the lowest R (0.31) and RMB (0.55) values. The unique basin topography was prone to cloudy weather, which may restrict the assimilation of MERRA-2 $\text{PM}_{2.5}$ products [37]. Generally, MERRA-2 produced lower daily mean $\text{PM}_{2.5}$ concentrations ($4.77\text{--}23.26 \mu\text{g m}^{-3}$) and the bias was more outstanding for high ground $\text{PM}_{2.5}$ ($>75 \mu\text{g m}^{-3}$). For instance, MERRA-2 $\text{PM}_{2.5}$ concentrations were entirely less than ground observations when $\text{PM}_{2.5} > 75 \mu\text{g m}^{-3}$. The lack of nitrate in the MERRA-2 $\text{PM}_{2.5}$ reanalysis would explain the underestimation [37,40]. In addition, to a certain extent, the bias caused by MERRA-2 AOD assimilation might be another reason for the MERRA-2 $\text{PM}_{2.5}$ underestimation, which will be verified in detail in the next section. Notably, in Figure 2d, no matter how large the ground $\text{PM}_{2.5}$ concentrations were, MERRA-2 $\text{PM}_{2.5}$ remained small. The reason might be that the unique basin terrain was prone to cloudy weather in the SB, and thus probably led to cloud screening bias for MERRA-2 aerosol reanalysis [8,9,40].

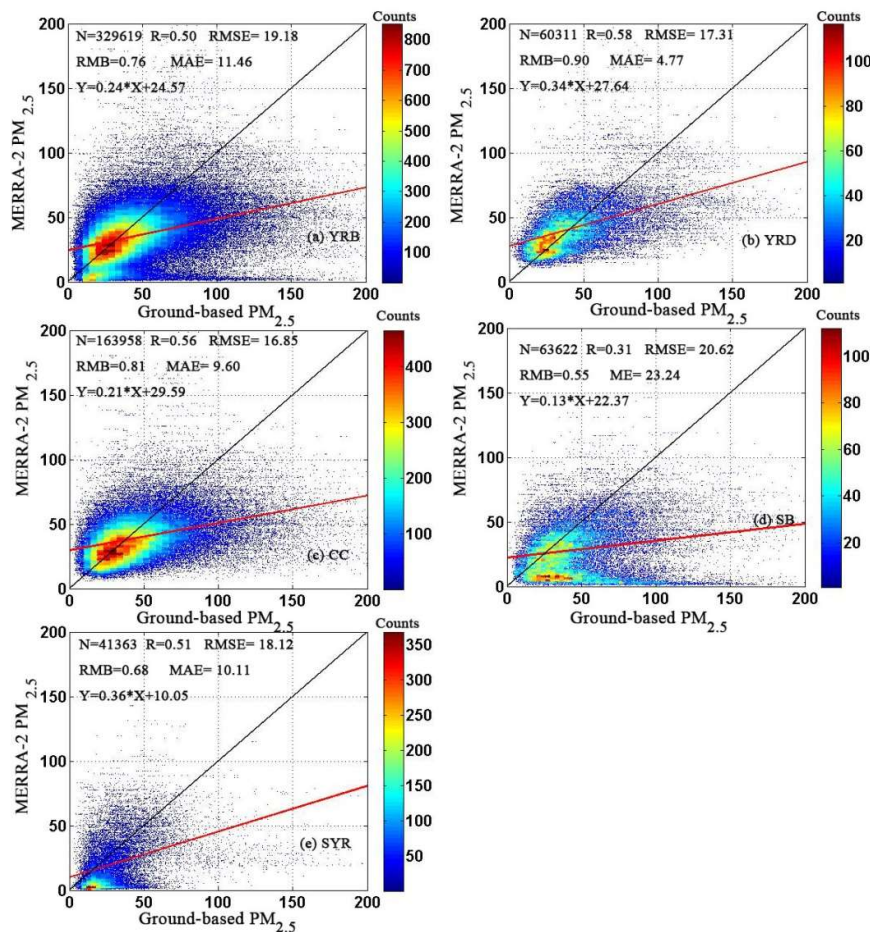


Figure 2. Scatter density maps between MERRA-2 and ground-based daily mean $PM_{2.5}$ concentrations over the (a) YRB, (b) YRD, (c) CC, (d) SB and (e) SYR for the period of Jan. 2015–Dec. 2016. The parameter N represents the number of matchups, R is the correlation coefficient, RMSE is the root mean square error, RMB is relative mean bias and MAE is the mean absolute error. The color bars represent the density of the matchups.

Figure 3 depicts the seasonal cycles of $PM_{2.5}$ concentrations from MERRA-2 reanalysis data and ground measurements. The seasonal comparison between the MERRA-2 and ground $PM_{2.5}$ was calculated as follows. First, according to Figure 1, the YRB was divided into four sub-regions including the YRD, CC, SB and SYR, with 87, 233, 95 and 60 state-controlled air quality monitoring stations, respectively. Then, based on the arithmetic averaging method, the seasonal average ground-based $PM_{2.5}$ concentrations in each sub-region were calculated by the daily average $PM_{2.5}$ from state-controlled air quality monitoring stations. Finally, the daily mean grid values of MERRA-2 $PM_{2.5}$ where the ground site was located were extracted from the MERRA-2 satellite images. Similarly, the seasonal average MERRA-2 $PM_{2.5}$ concentrations in each sub-region were calculated by the arithmetic averaging method. Results showed that both $PM_{2.5}$ products had similar seasonal variations in all regions, with high values in winter and low values in summer. Additionally, the bias also exhibited seasonal dependence. MERRA-2 $PM_{2.5}$ matched better with ground observations in summer, when the biases were only $4.16 \mu g m^{-3}$ (YRD), $-1.07 \mu g m^{-3}$ (CC), $-9.55 \mu g m^{-3}$ (SB), $-5.39 \mu g m^{-3}$ (SYR) and $-2.31 \mu g m^{-3}$ (YRB). The largest biases were observed in winter, reaching $-15.83 \mu g m^{-3}$ (YRD), $-27.45 \mu g m^{-3}$ (CC), $-43.73 \mu g m^{-3}$ (SB), $-19.77 \mu g m^{-3}$ (SYR) and $-27.67 \mu g m^{-3}$ (YRB). Similar comparison results were also reported over America [37] and the North China plain [40].

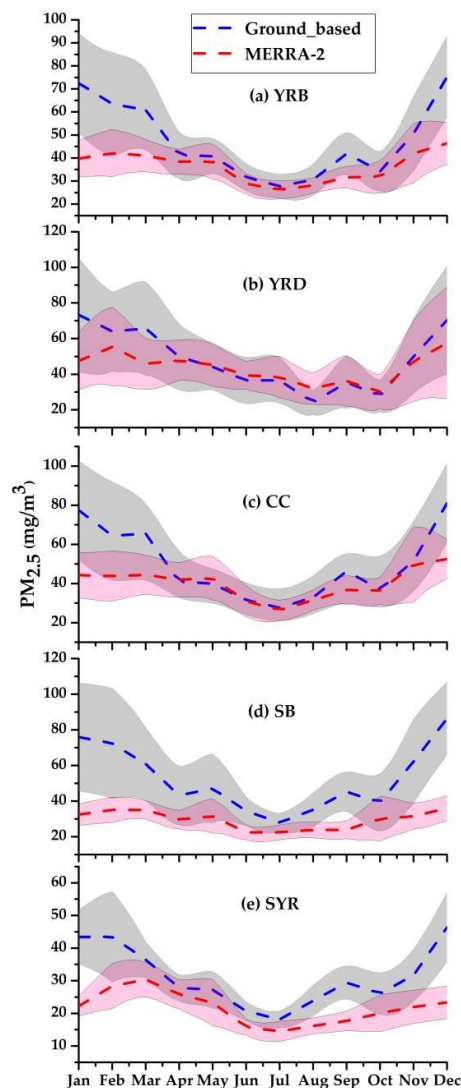


Figure 3. Monthly variations in $PM_{2.5}$ concentrations derived from MERRA-2 (red dashed lines) reanalysis and ground sites (blue dashed lines) over the (a) YRB, (b) YRD, (c) CC, (d) SB and (e) SYR for the period of Jan. 2015–Dec. 2016. The shading represents the standard deviation of MERRA-2 (red) and ground-based $PM_{2.5}$ (gray).

3.1.2. Impact of AOD Assimilation

Here, the effect of MERRA-2 AOD assimilation on the $PM_{2.5}$ simulation was estimated. Since there were no CARSNET AOD observations in the MERRA-2 aerosol assimilation, we compared daily mean MERRA-2 AOD with those ground measurements from five CARSNET sites of the YRB during 2013–2016 (Figure 4). As shown in Figure 4a, although MERRA-2 AOD was in good agreement with CARSNET AOD ($R = 0.82$), approximately 19% of MERRA-2 AOD were still underestimated, especially when CARSNET AOD > 1.0 . This was further confirmed by Figure 4b. The high MERRA-2 AOD values in Wuhan and Chengdu (> 0.8) were all below their corresponding CARSNET observations. By contrast, Shangri-La with low mean AOD (< 0.2) exhibited a good performance. Compared with the remote site of Shangri-La, Wuhan and Chengdu were two urban CARSNET sites with more complex aerosol sources and more diverse underlying surfaces, probably restraining the assimilation of the MERRA-2 AOD reanalysis [37,40]. Overall, the underestimation of MERRA-2 $PM_{2.5}$ was partly attributed to the negative bias of MERRA-2 AOD used in the GOCART model.

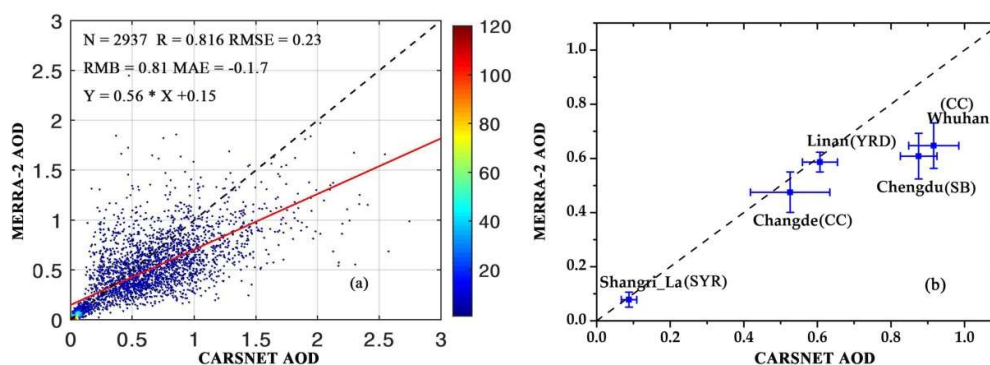


Figure 4. Scatter plot of daily averaged (a) and annual mean AOD (b) between MERRA-2 and CARSNET AOD at five ground sites of the YRB during 2013–2016. In (b), the vertical and horizontal bars refer to the standard deviations of the annual mean MERRA-2 and CARSNET AOD, respectively.

Figure 5 depicts AOD daily variations from Aqua, Terra, CARSNET and MERRA-2 products at Wuhan. As shown in Figure 5a, SO_4 dominated the aerosol types of Wuhan for the whole year. All AOD products showed similar daily variations, i.e., high values approximately occurred between the 50th and the 150th days. In addition, both satellite (Aqua and Terra) and ground (CARSNET) AOD observations were higher than MERRA-2 AODs. Additionally, it is worth noting that neither the satellites nor sun-photometer provided continuous AOD observations, especially during a heavy pollution episode (Figure 5b). This would make the assimilation of MERRA-2 AOD impossible, implying that the GOCART model for simulating aerosols in MERRA-2 needed further improvement.

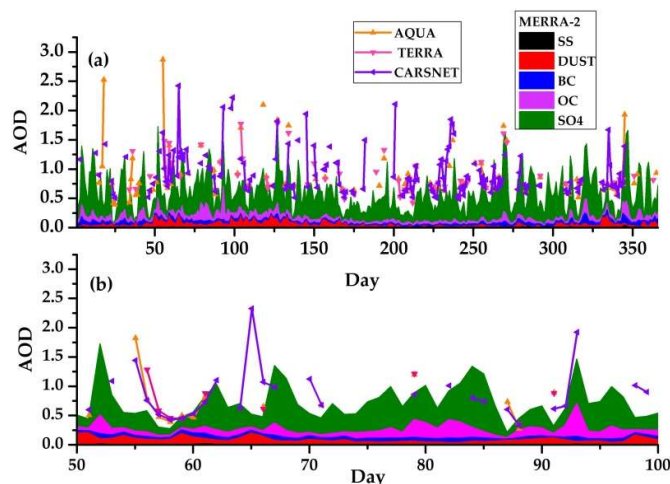


Figure 5. (a) Daily variations in AOD from satellite retrievals (Aqua and Terra), ground observations (CARSNET) and MERRA-2 reanalysis at Wuhan in 2016. The contributions of each aerosol species derived from MERRA-2 reanalysis are also shown. (b) Daily variations in AOD during a heavy pollution episode.

3.2. Spatiotemporal Distribution of MERRA-2 $\text{PM}_{2.5}$ Components

3.2.1. Annual Mean Distribution in MERRA-2 $\text{PM}_{2.5}$ Components

$\text{PM}_{2.5}$ components varied by region due to differences in anthropogenic emissions and meteorological conditions. The spatial distributions of annual mean MERRA-2 $\text{PM}_{2.5}$ components were illustrated in Figure 6. In Figure 6a, high $\text{PM}_{2.5}$ concentrations were observed over the YRD, CC and SB, while low values were concentrated in the SYR. A similar spatial pattern of $\text{PM}_{2.5}$ was also confirmed by the GWR $\text{PM}_{2.5}$ (Figure A2). Previous studies reported that GWR $\text{PM}_{2.5}$ reanalysis yielded good performance relative to ground observations [41,42]. Therefore, we used it here to verify

the spatial distribution of MERRA-2 PM_{2.5} reanalysis. According to the ambient air quality standard established by the World Health Organization (WHO), the annual mean PM_{2.5} concentration should not exceed 10 µg/m³ [23]. Approximately 67.49% and 78.27% of the pixels in the YRB exceeded the threshold for MERRA-2 and GWR, respectively (Figure A2). This fact suggested that it was necessary to clarify the composition of PM_{2.5} and its influencing factors over the YRB.

In terms of each PM_{2.5} component, sulfate PM_{2.5} (SO₄) occupied an average of 39.87% of the PM_{2.5} concentration, and its high values were concentrated in YRD, CC and SB. Similarly, high carbonaceous PM_{2.5} concentrations (BC and OC) were also observed in those regions, accounting for 8.02% and 28.32% of the PM_{2.5} concentrations, respectively. Emissions from power plants, vehicle exhaust and biomass burning could certainly explain the high PM_{2.5} concentrations in those areas. For dust PM_{2.5} (Dust_{2.5}), it accounted for 22.75% of the PM_{2.5} on average. In particular, high Dust_{2.5} concentrations appeared in the northern part of the YRB, which primarily came from local arid sources. Another region with high Dust_{2.5} concentrations was the SYR, possibly due to dust transportation from the Taklimakan desert in summer [7,8,43]. MERRA-2 sea salt PM_{2.5} (SS_{2.5}) constituted the lowest proportion of the total (approximately 1.02%), and rarely penetrated into land.

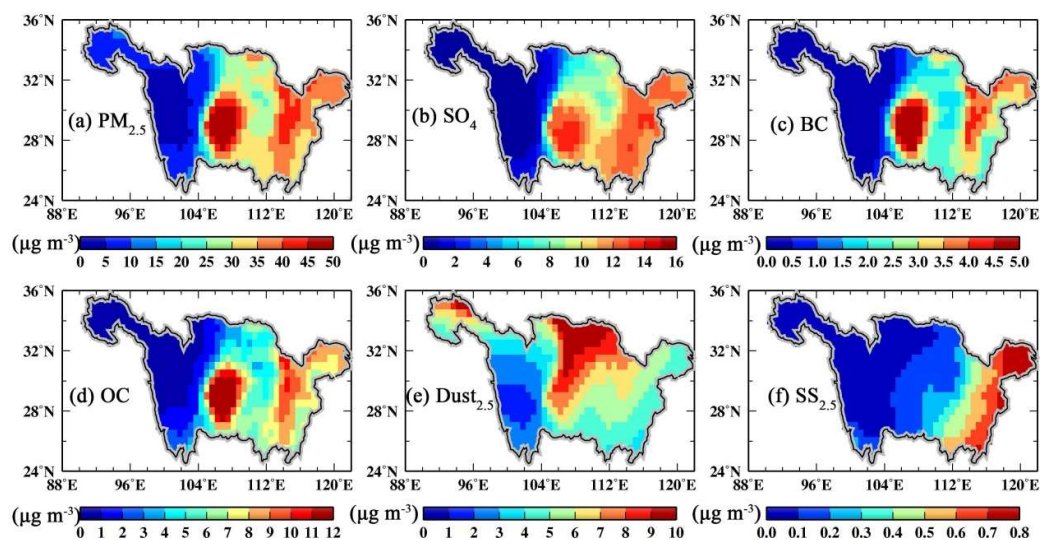


Figure 6. Annual mean distributions of each MERRA-2 PM_{2.5} component, including (a) the PM_{2.5}, (b) Sulfate PM_{2.5}, (c) Black Carbon PM_{2.5}, (d) Organic Carbon PM_{2.5}, (e) Dust PM_{2.5} and (f) Sea Salt PM_{2.5} over the YRB during 1980–2017.

3.2.2. Seasonal Variation in MERRA-2 PM_{2.5} Components

Figures 7 and 8 showed the spatial and seasonal differences of each PM_{2.5} component. A significant seasonal variation of PM_{2.5} was observed over the YRB, especially over the YRD, CC and SB. On average, its highest concentration of 26.63 µg m⁻³ occurred in winter and the lowest, 18.47 µg m⁻³, appeared in summer (Table 3). This was associated with the prevailing local monsoon climate [31]. In summer, windy and rainy weather was conducive to scavenging PM_{2.5} particles from the atmosphere, whereas the dry weather affected by the Mongolian anticyclone in winter prevented the diffusion of aerosol particles. The increase in emissions caused by heating in winter could certainly be another reason for the high PM_{2.5} concentration [31]. For each PM_{2.5} component, seasonal variations in SO₄, BC and OC were consistent with those of PM_{2.5}. Nevertheless, SS_{2.5} witnessed little seasonal changes over the YRB. Dust_{2.5} concentration was highest in spring (8.63 µg m⁻³), and most occurred in northern parts of the YRB. This was related to frequent sandstorm events in spring [35,36].

Table 3. Annual and seasonal mean values of each PM_{2.5} component over the YRB during 1980–2017, in units of $\mu\text{g m}^{-3}$.

	PM _{2.5}	SO ₄	BC	OC	Dust _{2.5}	SS _{2.5}
Annual	23.43	6.80	1.88	4.74	5.33	0.24
MAM	26.00	6.75	1.68	4.85	8.63	0.26
JJA	18.47	5.47	1.44	4.16	3.45	0.23
SON	22.63	7.13	1.98	4.45	4.37	0.24
DJF	26.63	7.83	2.42	5.50	4.88	0.23

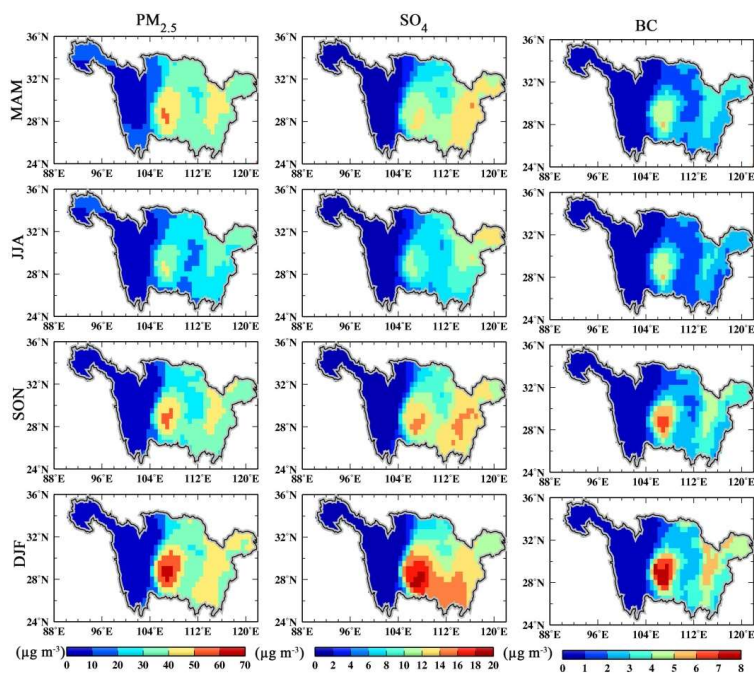


Figure 7. Seasonal variations of each MERRA-2 PM_{2.5} component: (left) the PM_{2.5}, (middle) SO₄ and (right) BC over the YRB during 1980–2017.

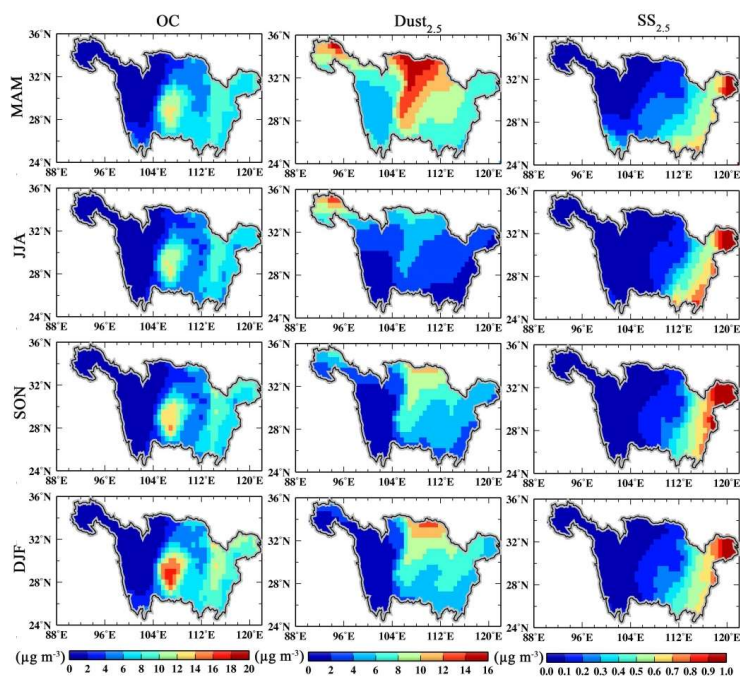


Figure 8. Seasonal variations of each MERRA-2 PM_{2.5} component: (left) OC, (middle) Dust_{2.5} and (right) SS_{2.5}.

3.2.3. Long-Term Trends of MERRA-2 PM_{2.5} Components

Figure 9 exhibited the interannual variability of each MERRA-2 PM_{2.5} component over the YRB during 1980–2017. A significant increasing trend of $11.4\text{E-}4 \mu\text{g m}^{-3} \text{ yr}^{-1}$ was observed in PM_{2.5} for the whole period. Notably, the growth trend of PM_{2.5} was effectively curbed after 2007. To reduce the uncertainty in the MERRA-2 PM_{2.5} trend, we also compared it with the interannual variability of GWR PM_{2.5} from 1998 to 2017 (Figure A3). The results showed that both PM_{2.5} products had similar growth trends, and there was a significant turning point from increasing to decreasing around 2007–2009. Similarly, He et al. [10] revealed that an over-increasing trend in MERRA-2 AOD over the YRB was curbed after 2008. The reason was probably due to the effective implementation of energy conservation and emission reduction policies in China [10]. Comparable trends were also found in SO₄, BC and OC, confirming that reduction in anthropogenic emissions was the dominant factor for the improvement in air quality. In addition, Dust_{2.5} and SS_{2.5} witnessed slightly increasing trends of $7.42\text{E-}5 \mu\text{g m}^{-3} \text{ yr}^{-1}$ and $1.63\text{E-}5 \mu\text{g m}^{-3} \text{ yr}^{-1}$ after 1980, respectively. Nevertheless, whether meteorological factors impacted air quality requires further analysis.

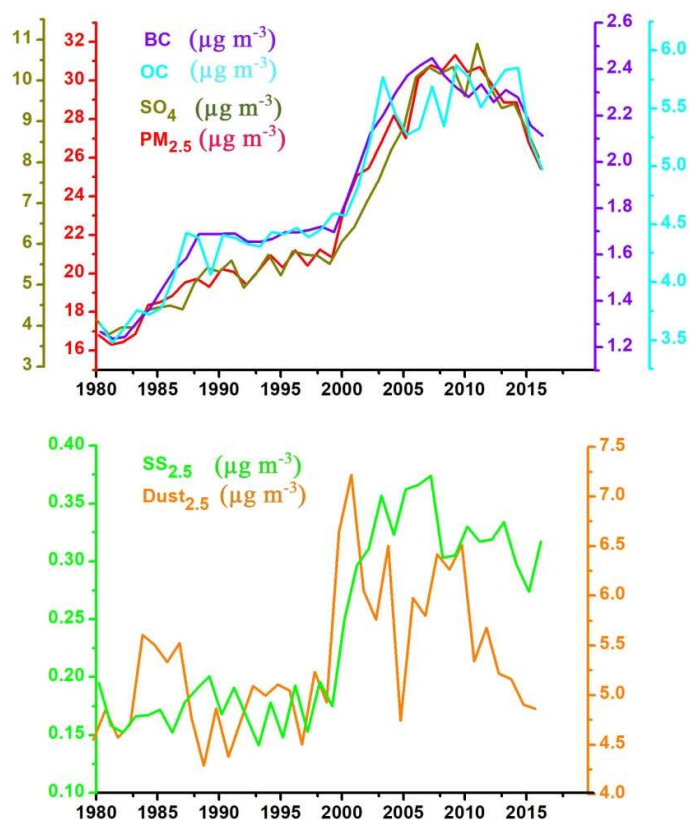


Figure 9. Annual mean trends in MERRA-2 PM_{2.5} and its five major components over the YRB from 1980 to 2017, in units of $\mu\text{g m}^{-3}$.

The annual mean trends of each MERRA-2 PM_{2.5} component at grid level were estimated by a linear regression, and their corresponding significant levels were further calculated based on the MK method (Figure 10). Overall, a significant increasing trend in PM_{2.5} ($0.7 \mu\text{g m}^{-3} \text{ yr}^{-1}$) was observed over the YRD, CC and SB. However, GWR exhibited a significant decreasing trend in PM_{2.5} in the mountains of the northern YRB (Figure A4), which was not observed in MERRA-2 PM_{2.5}. Recent studies demonstrated that the decreasing PM_{2.5} trend in those regions might be a response to the implementation of forest ecology projects over the middle and upper reaches of the YRB since the 1990s [44]. In terms of each PM_{2.5} component, SO₄, BC and OC witnessed significant increases,

especially over the YRD, CC and SB. By contrast, significant growth trends in $\text{Dust}_{2.5}$ and $\text{SS}_{2.5}$ occurred over the SYR and the eastern coastal regions, respectively.

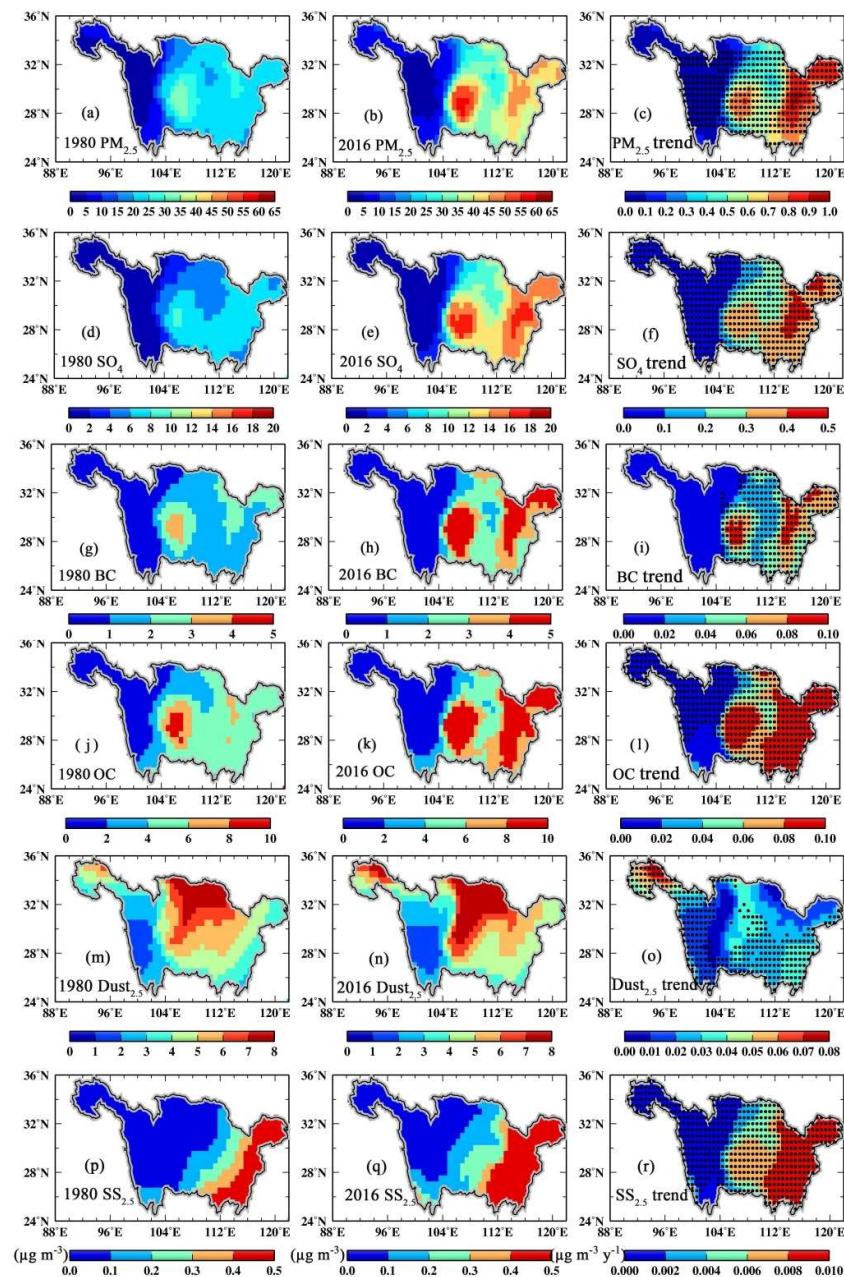


Figure 10. Spatial patterns of each MERRA-2 $\text{PM}_{2.5}$ component over the YRB from 1980 to 2017. The pixels marked with black dots represent significant trends ($p < 0.05$).

4. Discussion

To quantify the impact of meteorological variables on $\text{PM}_{2.5}$ changes, the slope coefficients β_i between daily mean $\text{PM}_{2.5}$ concentrations and six meteorological factors from 1980 to 2017 were calculated using the multiple linear regression (MLR) model (Equation (9)). Assuming that all other meteorological variables remained fixed, these slope coefficients actually represented the sensitivities of $\text{PM}_{2.5}$ to unit changes in each meteorological factor. In the MLR process, there should be no multicollinearity between the independent variables (i.e., meteorological factors), otherwise they would be eliminated [26,27]. In the correlation matrix (Table A1), even though there were several correlations of more than 0.5, most of them failed to pass the 95% significance test, indicating that

each meteorological variable was not significantly related to any other. Therefore, we concluded that collinearity was minimal and the MLR analysis could be performed. Figure 11 showed the adjusted coefficients of determination (adjusted- R^2) at grid level. Higher adjusted- R^2 values indicated that the MLR model performed better. The highest adjusted- R^2 values (~ 0.67) were mostly concentrated over the SYR, indicating that the local meteorological conditions could explain up to 67% of the daily $PM_{2.5}$ changes. By comparison, the values were lowest over the YRD and CC, where less than 20% of the daily $PM_{2.5}$ changes were due to meteorological variations. Over those regions, anthropogenic emissions from frequent industrialization and urbanization may be the major reason for high $PM_{2.5}$ concentrations. In Figure A5, adjusted- R^2 values showed seasonal variations, with high values (adjusted- $R^2 > 0.5$) in spring and summer over the SYR, suggesting that the local meteorological conditions could account for more than 50% of $PM_{2.5}$ changes. This may be closely related to the summer monsoon climate [26,27]. However, the relatively low adjusted- R^2 values (adjusted- $R^2 < 0.2$) dominated most areas of the YRB in autumn and winter. This may be due to an increase in anthropogenic emissions such as winter heating, which weakened the impact of meteorological conditions on air pollution in winter [26].

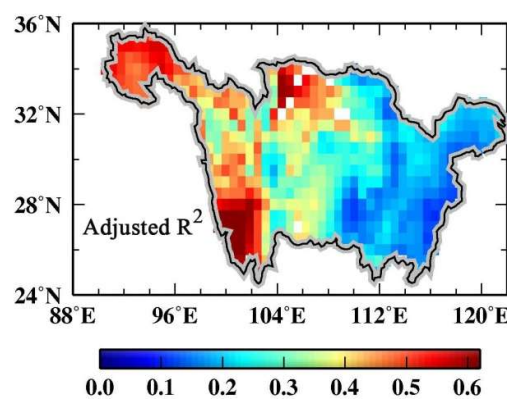


Figure 11. Coefficients of determination (R^2) of the MLR model between $PM_{2.5}$ and the six meteorological variables.

4.1. Sensitivity of $PM_{2.5}$ Components to Surface Wind Speed

Figure 12 depicts correlations of each $PM_{2.5}$ component with surface wind speed, as measured by the MLR regression coefficient (β_1) in Equation (9). Red grids represent positive correlations, whereas green grids are negative correlations. In Figure 12a, the $PM_{2.5}$ is significantly anti-correlated with surface wind speed throughout the YRB. High wind speeds facilitated circulation and dilution of aerosol particles, leading to a consistent decrease in $PM_{2.5}$. Negative correlations between $PM_{2.5}$ concentrations and surface wind speeds were also observed in the United States of America [26], Europe [27–29,31] and China [32–34]. Yang et al. [33] discovered a negative wind- $PM_{2.5}$ correlation throughout China except Hainan Island. Compared with the USA and Europe, China had the worst atmospheric dispersion conditions with annual stagnation frequency of 29%, leading to serious air pollutions especially in winter [31]. However, a significant positive correlation occurred in the SYR, where a plenty of dust particles were concentrated (see Section 3.2). It was probably due to the strong wind speed dependence of dust particles, further confirmed by the $Dust_{2.5}$ -wind regression in Figure 12e. Similarly, in Saudi Arabia (an arid region), both $PM_{2.5}$ and PM_{10} were positively related to wind speed [30]. Additionally, in Figure A6 and Table A2, most of the YRB experienced an average decrease of 0.05 m s^{-1} per year in wind speed from 1980 to 2017. Based on the MLR model, the average $PM_{2.5}$ -wind regression coefficient was approximately $-2.42 \mu\text{g m}^{-3} \text{ m}^{-1} \text{ s}$, leading to an average increase of $0.12 \mu\text{g m}^{-3}$ per year in $PM_{2.5}$ over the YRB. However, all other meteorological variables remained fixed (Table A2).

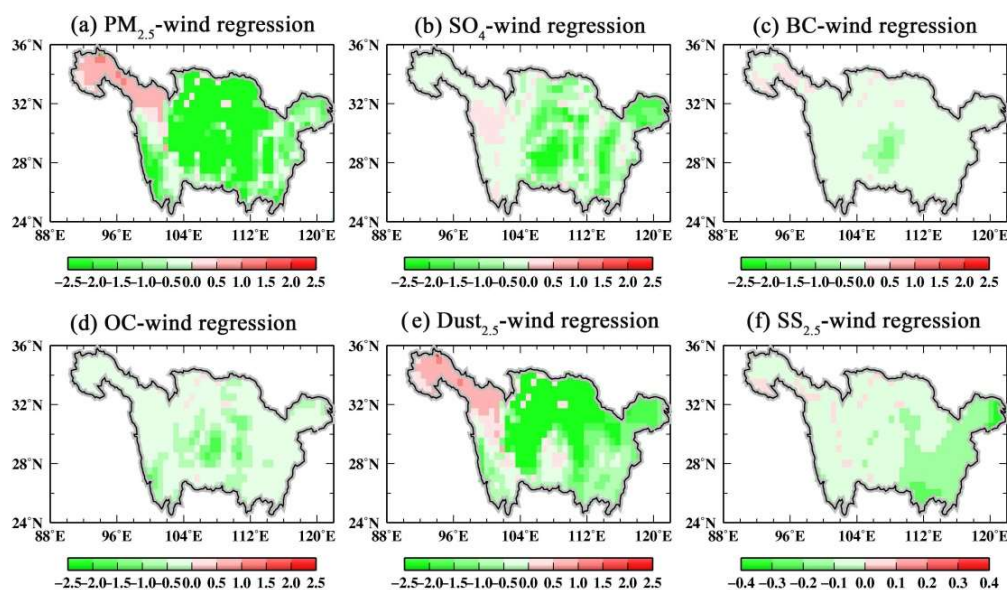


Figure 12. Multiple linear regression coefficients (β_1) of each $PM_{2.5}$ component with surface wind speed (Wind), in units of $\mu\text{g m}^{-3} \text{m}^{-1} \text{s}$. (a–f) refer to the regression coefficients of $PM_{2.5}$, SO_4 , BC, OC, $Dust_{2.5}$ and $SS_{2.5}$ with surface wind speed, respectively.

4.2. Sensitivity of $PM_{2.5}$ Components to Surface Temperature

In Figure 13, surface temperature (T) was significantly positively correlated with each $PM_{2.5}$ component across the YRB. Similar results were also reported on global [27] and regional [26] scales. Westervelt et al. [27] discovered a robust positive relationship between surface temperature and $PM_{2.5}$ throughout the continents and oceans except East and South Asia. This positive correlation may be related to temperature-dependent reaction rates and changes in oxidant abundance, that is, the oxidation of aerosol precursors (such as sulfur dioxide) could be enhanced with higher temperature [27]. However, in China, Yang et al. [33] revealed that surface temperature was negatively related to $PM_{2.5}$ in autumn but positively correlated with $PM_{2.5}$ in winter. Dawson et al. [45] found an averaged negative effect of temperature on $PM_{2.5}$ east of the USA, primarily due to the volatilization of nitrate at high temperature. Since nitrate aerosols were not assimilated in the MERRA-2 $PM_{2.5}$ reanalysis, there was little negative relationship between $PM_{2.5}$ and temperature over the YRB. In addition, Figure A6 and Table A2 showed an average increase of 0.03 K per year in temperature from 1980 to 2017. Based on the MLR model between temperature and the $PM_{2.5}$ (Figure 13a), the average sensitivity of $0.11 \mu\text{g m}^{-3} \text{K}^{-1}$ could lead to $PM_{2.5}$ growth of up to $0.003 \mu\text{g m}^{-3}$ per year. Overall, the temperature effect on $PM_{2.5}$ ($0.11 \mu\text{g m}^{-3} \text{K}^{-1}$) was weaker than the influence of wind speed ($-2.42 \mu\text{g m}^{-3} \text{m}^{-1} \text{s}$) over the YRB (Table A2).

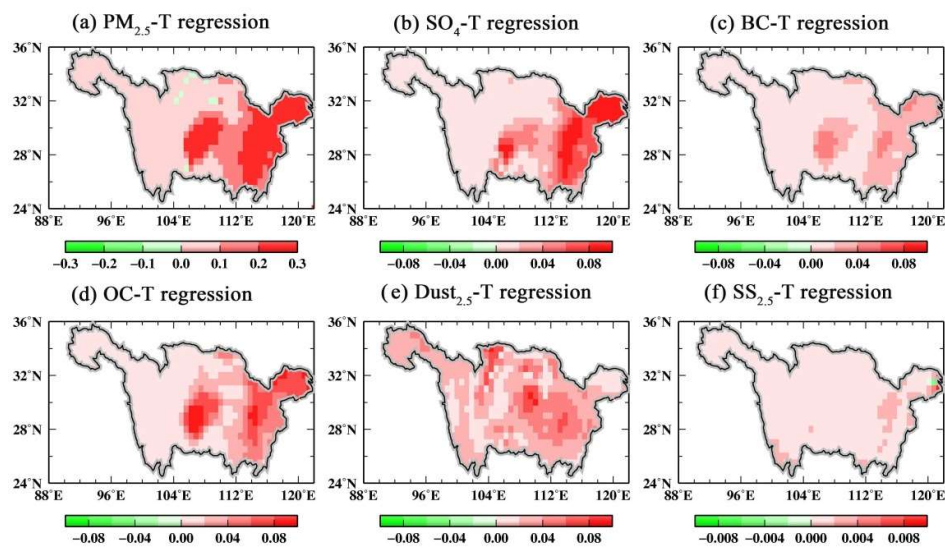


Figure 13. Multiple linear regression coefficients (β_2) of each $PM_{2.5}$ component with surface temperature (T), in units of $\mu\text{g m}^{-3} \text{K}^{-1}$. (a–f) refer to the regression coefficients of $PM_{2.5}$, SO_4 , BC, OC, $Dust_{2.5}$ and $SS_{2.5}$ with surface temperature, respectively.

4.3. Sensitivity of $PM_{2.5}$ Components to Precipitation

Figure 14 shows the slope coefficients between each $PM_{2.5}$ component and precipitation. Each $PM_{2.5}$ component was significantly anti-correlated with precipitation in most areas of the YRB, primarily due to wet scavenging [26–35]. However, a positive relationship was observed in the SYR, where dust particle was the main air pollutant (see Section 3.2) and precipitation did not occur frequently [46–48]. Even if there was a small amount of precipitation over the SYR, it may have only increased the relative humidity, resulting in the growth of hygroscopic particles [27]. Precipitation changes were typically more positive than negative from 1980 to 2017, along with an annual trend of 0.02 mm day^{-1} (Figure A6 and Table A2). Overall, based on the MLR model of $PM_{2.5}$ and precipitation (Figure 14a), the average sensitivity of $-0.34 \mu\text{g m}^{-3} \text{mm}^{-1} \text{day}$ could lead to a decrease of $0.007 \mu\text{g m}^{-3}$ per year for $PM_{2.5}$, which was comparable to the effect of temperature on $PM_{2.5}$ (Table A2).

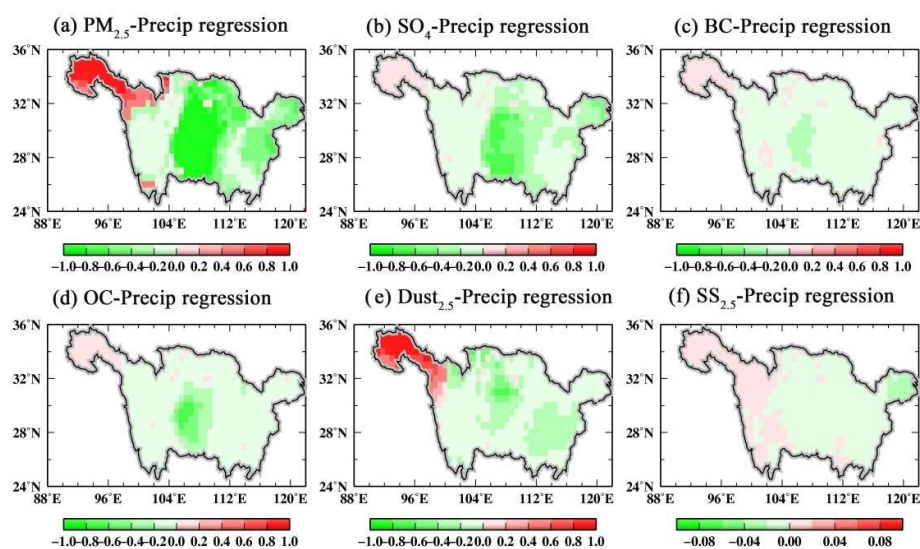


Figure 14. Multiple linear regression coefficients (β_3) of each $PM_{2.5}$ component with surface precipitation (Precip), in units of $\mu\text{g m}^{-3} \text{mm}^{-1} \text{day}$. (a–f) refer to the regression coefficients of $PM_{2.5}$, SO_4 , BC, OC, $Dust_{2.5}$ and $SS_{2.5}$ with precipitation, respectively.

4.4. Sensitivity of PM_{2.5} Components to Relative Humidity

Figure 15 shows the slope coefficients for each PM_{2.5} component and relative humidity (RH). As can be seen in Figure 15a, PM_{2.5} was positively correlated with RH in most areas of the YRB, with the exception of the YRD. Throughout the YRB, significant positive correlations with RH were also found in SO₄, BC and OC, likely due to the dependence of sulfate and carbonaceous PM_{2.5} formation on RH [26,27]. In contrast, Dust_{2.5} had an anti-correlation with RH, which probably explained the negative association of PM_{2.5} with RH in the YRD. Yang et al. [33] found a positive correlation between PM_{2.5} and RH in north China and a negative correlation in south China. A negative PM_{2.5}-RH regression was also estimated over the Pearl River Delta Region [34]. They considered that when RH was greater than 80%, rainfall often occurred, leading to a decrease in PM_{2.5} in the atmosphere [34]. In this study, YRD had a temperate monsoon climate, which made precipitation events occur in most days with high RH (>80%), especially in summer. Thus, there was a negative PM_{2.5}-RH regression over the YRD. However, with the relatively low slope coefficient for total PM_{2.5} and RH (0.05 $\mu\text{g m}^{-3} \%^{-1}$), the sensitivity of PM_{2.5} to RH was small (Table A2).

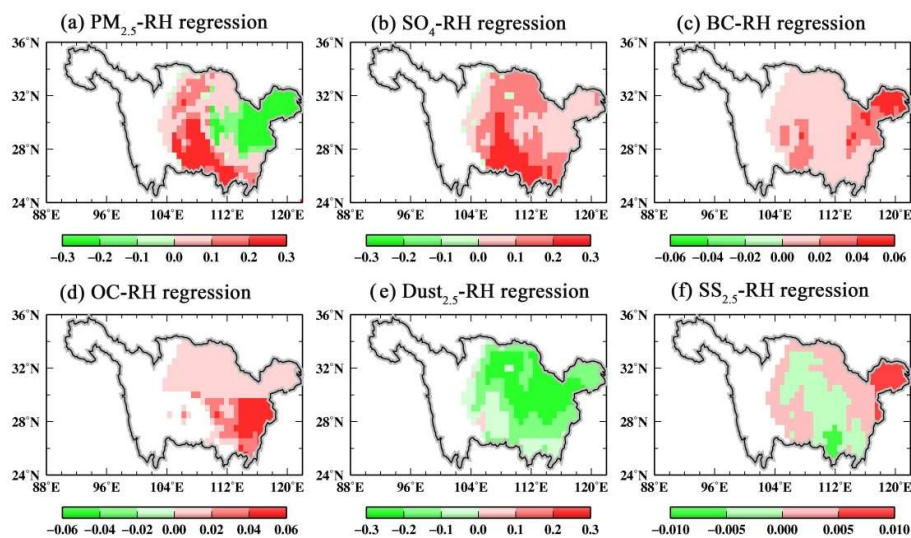


Figure 15. Multiple linear regression coefficients (β_4) of each PM_{2.5} component with relative humidity (RH), in units of $\mu\text{g m}^{-3} \%^{-1}$. The blank grids indicate invalid values. (a–f) refer to the regression coefficients of PM_{2.5}, SO₄, BC, OC, Dust_{2.5} and SS_{2.5} with relative humidity, respectively.

4.5. Sensitivity of PM_{2.5} Components to Total Cloud Cover

In Figure 16, anti-correlations between each PM_{2.5} component and the total cloud cover were observed mostly over the middle and lower reaches of the YRB. In those regions, clouds could partially prevent aerosol precursors (such as sulfur dioxide) from oxidizing, and thus, reduced PM_{2.5} concentrations in the atmosphere [27]. However, positive regressions between each PM_{2.5} component and the total cloud cover occurred in the SYR, possibly due to the enhancements in in-cloud production of sulfate aerosols. Overall, the average sensitivity of PM_{2.5} to the total cloud cover was approximately $-0.07 \mu\text{g m}^{-3} \%^{-1}$ (Figure 16a and Table A2).

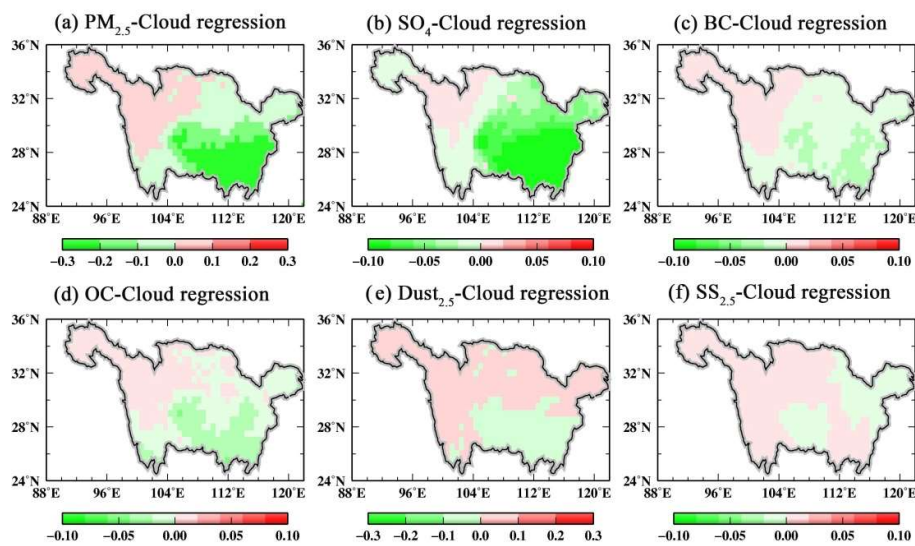


Figure 16. Multiple linear regression coefficients (β_5) of each $\text{PM}_{2.5}$ component with total cloud cover (cloud), in units of $\mu\text{g m}^{-3} \%^{-1}$. (a–f) refer to the regression coefficients of $\text{PM}_{2.5}$, SO_4 , BC, OC, $\text{Dust}_{2.5}$ and $\text{SS}_{2.5}$ with total cloud cover, respectively.

4.6. Sensitivity of $\text{PM}_{2.5}$ Components to Boundary Layer Height

In Figure 17, the relationship of each $\text{PM}_{2.5}$ component with boundary layer height (BLH) was robustly negative throughout the YRB. The reason may be that a well-developed BLH was conducive to the diffusion and dilution of $\text{PM}_{2.5}$ particles [31]. Recently, Wang et al. [31] reported that BLH was lower than the normal during heavy pollution in Beijing, China. During 1980–2017, the YRB experienced a significant decrease of -0.98 m per year in BLH, especially over the YRD, CC and SB (Figure A6). Based on the MLR model between BLH and $\text{PM}_{2.5}$ (Figure 17a and Table A2), the average sensitivity of $0.006 \mu\text{g m}^{-3} \text{m}^{-1}$ could lead to $\text{PM}_{2.5}$ growth of up to $0.006 \mu\text{g m}^{-3}$ per year.

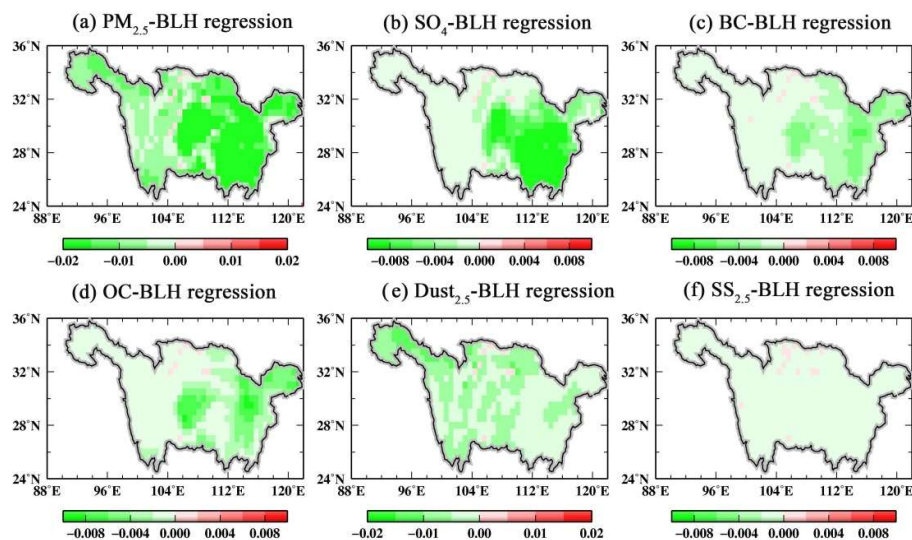


Figure 17. Multiple linear regression coefficients (β_6) of each $\text{PM}_{2.5}$ component with boundary layer height (BLH), in units of $\mu\text{g m}^{-3} \text{m}^{-1}$. (a–f) refer to the regression coefficients of $\text{PM}_{2.5}$, SO_4 , BC, OC, $\text{Dust}_{2.5}$ and $\text{SS}_{2.5}$ with boundary layer height, respectively.

5. Conclusions

Based on the MLR model, the sensitivities of $\text{PM}_{2.5}$ and its major components to meteorological variables were quantified using daily mean MERRA-2 $\text{PM}_{2.5}$ and meteorology reanalysis data over the

YRB from 1980 to 2017. First of all, in order to verify the accuracy of the MERRA-2 PM_{2.5} reanalysis, it was compared with ground-based measurements derived from 476 air quality monitoring sites in the YRB. The results suggested that MERRA-2 PM_{2.5} was underestimated relative to their corresponding ground observations throughout the YRB. In addition to the lack of nitrate aerosols in GOCART, the bias in MERRA-2 AOD assimilation could also partly explain the underestimation of MERRA-2 PM_{2.5}.

The YRB witnessed severe air pollution, with its annual mean PM_{2.5} concentration of 23.43 $\mu\text{g m}^{-3}$. In particular, approximately 67.49% of the pixels in the YRB exceeded the annual mean threshold of 10 $\mu\text{g m}^{-3}$ recommended by the WHO. The high PM_{2.5} concentrations were observed over the YRD, CC and SB in winter, while the low values occurred in the SYR in summer. For each PM_{2.5} component, SO₄, BC and OC showed similar spatiotemporal distributions with PM_{2.5} concentration. The temperate monsoon climate could account for the seasonal and spatial variations of PM_{2.5} concentrations in the YRB. However, Dust_{2.5} had the highest concentrations of 8.63 $\mu\text{g m}^{-3}$ over the SYR and the northern areas of the YRB in spring, which came from local arid sources. Most of the SS_{2.5} were concentrated in the eastern coastal areas and there was no significant seasonal variation. Over-increasing trends (1980 onward) in all PM_{2.5} components were confirmed in the YRB; however, they were curbed after 2007.

Based on the MLR model, we found the highest adjusted-R² (0.67) in the SYR, suggesting that the six meteorological variables could explain up to 67% of the daily PM_{2.5} changes in that region. Furthermore, each PM_{2.5} component was significantly anti-correlated with surface wind speed and precipitation throughout the YRB. High wind speeds and precipitations facilitated the circulation and dilution of PM_{2.5} from the atmosphere. Nevertheless, a positive wind-PM_{2.5} regression was observed in the SYR, probably due to the dependence of Dust_{2.5} on wind. Furthermore, SYR witnessed a positive relationship between precipitation and PM_{2.5}, which was likely associated with an increase in relative humidity (RH). Additionally, boundary layer height (BLH) was robustly anti-correlated with each PM_{2.5} component. However, the impact of BLH on PM_{2.5} ($-0.006 \mu\text{g m}^{-3} \text{ m}^{-1}$) was far less than those of wind speed ($-2.42 \mu\text{g m}^{-3} \text{ m}^{-1} \text{ s}$) and precipitation ($-0.34 \mu\text{g m}^{-3} \text{ mm}^{-1} \text{ day}$). In contrast, surface temperature was positively correlated with each PM_{2.5} component across the YRB, and the sensitivity of PM_{2.5} to temperature was approximately $0.11 \mu\text{g m}^{-3} \text{ K}^{-1}$. This was possibly due to the enhancement in oxidation of aerosol precursors at high temperatures. The RH-PM_{2.5} regression showed regional dependencies, with negative correlation in the YRD and positive correlation in the other areas. A negative relationship between total cloud cover and PM_{2.5} occurred in the middle and lower reaches of the YRB. However, the sensitivities of PM_{2.5} to RH ($0.05 \mu\text{g m}^{-3} \%^{-1}$) and total cloud cover ($0.07 \mu\text{g m}^{-3} \%^{-1}$) were relatively small. Overall, this study highlighted the impact of meteorological conditions on PM_{2.5}, even though it was relatively minor in comparison with the anthropogenic emissions effect [27]. When assessing the effects of emission reductions and further formulating mitigation policies, the unfavorable atmospheric diffusion conditions should not be ignored in China.

Author Contributions: L.H. designed the research; H.Z., Z.Z., X.C. and L.H. performed the experiments and analyzed the data; L.H. He wrote the manuscript; A.L. and P.H. revised the manuscript.

Funding: This work was financially supported by National Major Scientific Instruments and Equipment Development Project (2012YQ10022507), National Natural Science Foundation of China (No.41601044, No.41571400, No. 41704012), the Special Fund for Basic Scientific Research of Central Colleges, China University of Geosciences, Wuhan (No. CUG150631, CUGL170401, CUGCJ1704).

Conflicts of Interest: The authors declare no conflict of interest.

Appendix A

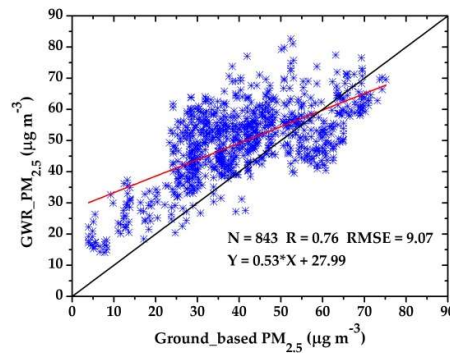


Figure A1. Scatter plot between GWR and ground-based annual mean $PM_{2.5}$ concentrations derived from 476 air quality monitoring stations of the YRB for the period of Jan. 2015–Dec. 2016. The black line is a 1:1 line and the red line is a linear fit line.

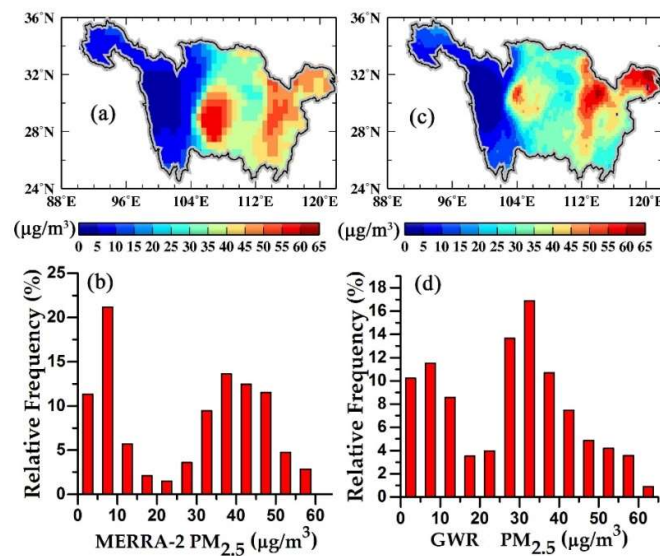


Figure A2. The spatial (top) and frequency (bottom) distributions of multiyear-averaged surface $PM_{2.5}$ concentrations derived from MERRA-2 (a,b), GWR-1 (c,d) over the YRB for the period of 1998–2016.

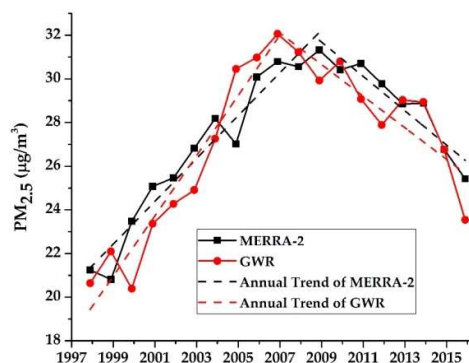


Figure A3. Temporal variations of annual mean $PM_{2.5}$ concentration derived from MERRA-2 (black) and GWR (red) over the YRB from 1998 to 2016.

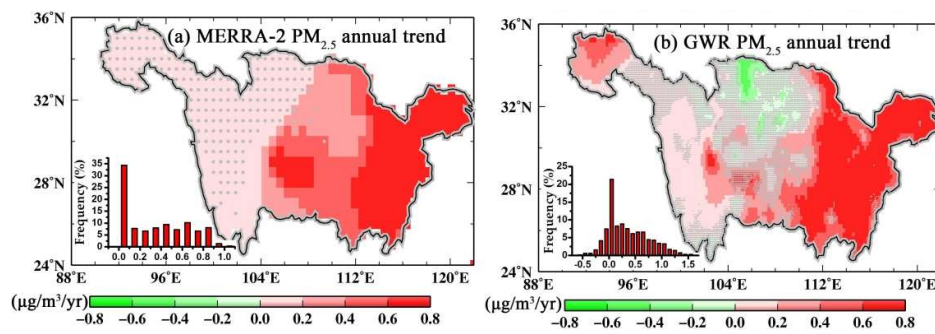


Figure A4. Spatial distribution of PM_{2.5} annual trend derived from MERRA-2 (a) and GWR (b) over the YRB from 1998 to 2016. Grids marked by grey points represented PM_{2.5} trends that did not exceed a 95% significant level.

Table A1. Correlation matrix between meteorological variables temperature (T), precipitation (Precip), total cloud cover (Cloud), wind speed (Wind), relative humidity (RH) and Boundary layer height (BLH). * represents *p*-value < 0.05.

	T	Wind	Precip	RH	Cloud	BLH
T	1					
Wind	0.514	1				
Precip	-0.202	-0.089	1			
RH	0.074	-0.334	0.359	1		
Cloud	0.274	0.26	0.519 *	0.28	1	
BLH	-0.559	-0.543	-0.222	0.351	-0.416	1

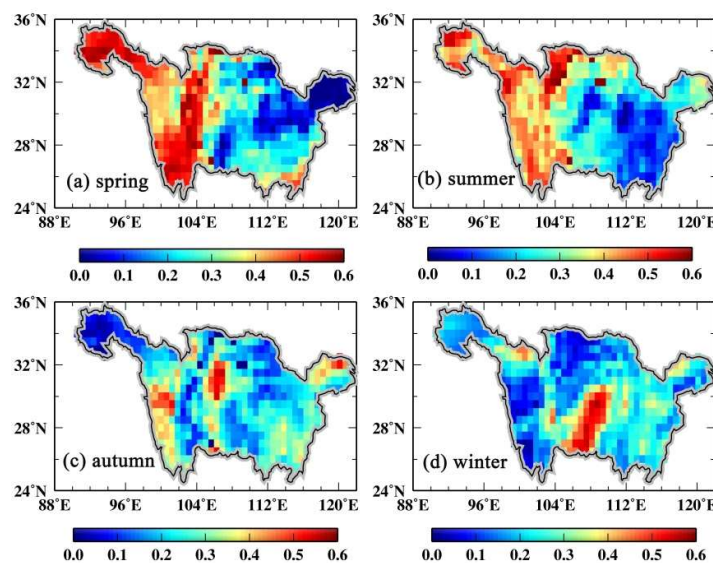


Figure A5. Coefficients of determination (R^2) of the MLR model between PM_{2.5} and the six meteorological variables in spring (a), summer (b), autumn (c) and winter (d).

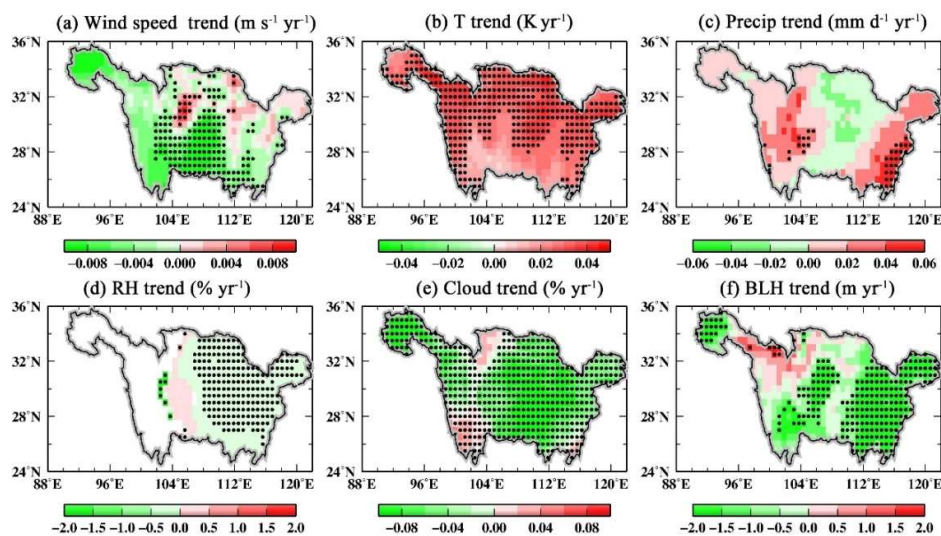


Figure A6. Annual trends in meteorological factors over the YRB from 1980 to 2017.

Table A2. Summary of regression coefficients between surface $PM_{2.5}$ and meteorological variables, annual trends in meteorological variables and theoretical annual trends in $PM_{2.5}$ based on MLR model. $\beta_1 \dots \beta_6$ refer to regression coefficients between $PM_{2.5}$ and wind speed (Wind), temperature (T), precipitation (Precip), relative humidity (RH), total cloud cover (Cloud) and Boundary layer height (BLH), respectively.

Regression Coefficients	Annual trends in Meteorological Variables	Theoretical Annual Trends in $PM_{2.5}$
β_1 ($-2.42 \mu\text{g m}^{-3} \text{ m}^{-1} \text{ s}$)	Wind (0.05 m s^{-1})	$0.12 \mu\text{g m}^{-3}$
β_2 ($0.11 \mu\text{g m}^{-3} \text{ K}^{-1}$)	T (0.03 K)	$0.003 \mu\text{g m}^{-3}$
β_3 ($-0.34 \mu\text{g m}^{-3} \text{ mm}^{-1} \text{ day}$)	Precip (0.02 mm day^{-1})	$0.007 \mu\text{g m}^{-3}$
β_4 ($0.05 \mu\text{g m}^{-3} \%^{-1}$)	RH (-0.16%)	$-0.008 \mu\text{g m}^{-3}$
β_5 ($-0.07 \mu\text{g m}^{-3} \%^{-1}$)	Cloud (-0.05%)	$0.0004 \mu\text{g m}^{-3}$
β_6 ($0.006 \mu\text{g m}^{-3} \text{ m}^{-1}$)	BLH (-0.98 m)	$0.006 \mu\text{g m}^{-3}$

References

- IPCC. Climate change 2013: the physical science basis. In *Contribution of Working Group I to the Fifth Assessment Report of the Intergovernmental Panel on Climate Change*; Stocker, T.F., Qin, D., Plattner, G.-K., Tignor, M., Allen, S.K., Boschung, J., Nauels, A., Xia, Y., Bex, V., Midgley, P.M., Eds.; Cambridge University Press: Cambridge, UK; New York, NY, USA, 2013; p. 1535.
- Guo, J.; Xia, F.; Zhang, Y.; Liu, H.; Li, J.; Lou, M.; Zhai, P. Impact of diurnal variability and meteorological factors on the $PM_{2.5}$ -AOD relationship: Implications for $PM_{2.5}$ remote sensing. *Environ. Pollut.* **2017**, *221*, 94–104. [[CrossRef](#)] [[PubMed](#)]
- He, J.; Gong, S.; Yu, Y.; Yu, L.; Wu, L.; Mao, H.; Li, R. Air pollution characteristics and their relation to meteorological conditions during 2014–2015 in major Chinese cities. *Environ. Pollut.* **2017**, *223*, 484–496. [[CrossRef](#)] [[PubMed](#)]
- Zhang, M.; Wang, L.; Gong, W.; Ma, Y.; Liu, B. Aerosol optical properties and direct radiative effects over Central China. *Remote Sens.* **2017**, *9*, 997. [[CrossRef](#)]
- Zhang, M.; Ma, Y.; Wang, L.; Gong, W.; Hu, B.; Shi, Y. Spatial-temporal characteristics of aerosol loading over the Yangtze River Basin during 2001–2015. *Int. J. Climatol.* **2018**, *38*, 2138–2152. [[CrossRef](#)]
- Qin, W.; Liu, Y.; Wang, L.; Lin, A.; Xia, X.; Che, H.; Zhang, M. Characteristic and driving factors of aerosol optical depth over mainland China during 1980–2017. *Remote Sens.* **2018**, *10*, 1064. [[CrossRef](#)]
- Lelieveld, J.; Evans, J.S.; Fnais, M.; Giannadaki, D.; Pozzer, A. The contribution of outdoor air pollution sources to premature mortality on a global scale. *Nature* **2015**, *525*, 367–371. [[CrossRef](#)] [[PubMed](#)]
- He, L.; Wang, L.; Lin, A.; Zhang, M.; Bilal, M.; Tao, M. Aerosol Optical Properties and Associated Direct Radiative Forcing over the Yangtze River Basin during 2001–2015. *Remote Sens.* **2017**, *9*, 746. [[CrossRef](#)]

9. He, L.; Wang, L.; Lin, A.; Zhang, M.; Bilal, M.; Wei, J. Performance of the NPP-VIIRS and aqua-MODIS Aerosol Optical Depth Products over the Yangtze River Basin. *Remote Sens.* **2018**, *10*, 117. [[CrossRef](#)]
10. He, L.; Wang, L.; Lin, A.; Zhang, M.; Xia, X.; Tao, M.; Zhou, H. What drives changes in aerosol properties over the Yangtze River Basin in past four decades? *Atmos. Environ.* **2018**, *190*, 269–283. [[CrossRef](#)]
11. Wang, L.; Gong, W.; Xia, X.; Zhu, J.; Li, J.; Zhu, Z. Long-term observations of aerosol optical properties at Wuhan, an urban site in Central China. *Atmos. Environ.* **2015**, *101*, 94–102. [[CrossRef](#)]
12. Che, H.; Xia, X.; Goloub, P.; Holben, B.; Zhao, H.; Wang, Y.; Zhang, X.; Wang, H.; Blarel, L.; Damiri, B. Ground-based aerosol climatology of China: aerosol optical depths from the China Aerosol Remote Sensing Network (CARSNET) 2002-2013. *Atmos. Chem. Phys.* **2015**, *15*, 7619–7652. [[CrossRef](#)]
13. Wei, J.; Sun, L. Comparison and evaluation of different modis aerosol optical depth products over the beijing-tianjin-hebei region in china. *IEEE J-STARs* **2016**, *PP(99)*, 1–10. [[CrossRef](#)]
14. Wang, L.; Lu, Y.; Zou, L.; Feng, L.; Wei, J.; Qin, W.; Niu, Z. Prediction of diffuse solar radiation based on multiple variables in China. *Renew. Sust. Energ. Rev.* **2019**, *103*, 151–216. [[CrossRef](#)]
15. Feng, L.; Lin, A.; Wang, L.; Qin, W.; Gong, W. Evaluation of sunshine-based models for predicting diffuse solar radiation in China. *Renew. Sust. Energ. Rev.* **2018**, *94*, 168–182. [[CrossRef](#)]
16. Feng, L.; Qin, W.; Wang, L.; Lin, A.; Zhang, M. Comparison of Artificial Intelligence and Physical Models for Forecasting Photosynthetically-Active Radiation. *Remote Sens.* **2018**, *10*, 1855. [[CrossRef](#)]
17. Wang, L.; Chen, Y.; Niu, Y.; Salazar, G.A.; Gong, W. Analysis of atmospheric turbidity in clear skies at Wuhan, Central China. *J. Earth Sci.* **2017**, *28*, 729–738. [[CrossRef](#)]
18. Wang, L.; Kisi, O.; Zounemat-Kermani, M.; Zhu, Z.; Gong, W.; Niu, Z.; Liu, Z. Prediction of solar radiation in China using different adaptive neuro-fuzzy methods and M5 model tree. *Int. J. Climatol.* **2017**, *37*, 1141–1155. [[CrossRef](#)]
19. Wang, L.; Kisi, O.; Zounemat-Kermani, M.; Salazar, G.A.; Zhu, Z.; Gong, W. Solar radiation prediction using different techniques: model evaluation and comparison. *Renew. Sust. Energ. Rev.* **2016**, *61*, 384–397. [[CrossRef](#)]
20. Zhang, M.; Ma, Y.; Gong, W.; Wang, L.; Xia, X.; Che, H.; Hu, B.; Liu, B. Aerosol radiative effect in UV, VIS, NIR, and SW spectra under haze and high-humidity urban conditions. *Atmos. Environ.* **2017**, *166*, 9–21. [[CrossRef](#)]
21. Guo, J.; He, J.; Liu, H.; Miao, Y.; Liu, H.; Zhai, P. Impact of various emission control schemes on air quality using WRF-Chem during APEC China 2014. *Atmos. Environ.* **2016**, *140*, 311–319. [[CrossRef](#)]
22. Ren, Y.; Li, H.; Meng, F.; Wang, G.; Zhang, H.; Yang, T.; Li, W.; Ji, Y.; Bi, F.; Wang, X. Impact of emission controls on air quality in Beijing during the 2015 China Victory Day Parade: Implication from organic aerosols. *Atmos. Environ.* **2019**, *198*, 207–214. [[CrossRef](#)]
23. Larkin, A.; Van Donkelaar, A.; Geddes, J.A.; Martin, R.V.; Hystad, P. Relationships between changes in urban characteristics and air quality in East Asia from 2000 to 2010. *Environ. Sci. Technol.* **2016**, *50*, 9142–9149. [[CrossRef](#)] [[PubMed](#)]
24. Li, T.; Wang, Y.; Zhao, D. Environmental Kuznets curve in China: new evidence from dynamic panel analysis. *Energy Policy* **2016**, *91*, 138–147. [[CrossRef](#)]
25. Liu, Y.; Zhou, Y.; Wu, W. Assessing the impact of population, income and technology on energy consumption and industrial pollutant emissions in China. *Appl. Energy* **2015**, *155*, 904–917. [[CrossRef](#)]
26. Tai, A.P.; Mickley, L.J.; Jacob, D.J. Correlations between fine particulate matter (PM_{2.5}) and meteorological variables in the United States: Implications for the sensitivity of PM_{2.5} to climate change. *Atmos. Environ.* **2010**, *44*, 3976–3984. [[CrossRef](#)]
27. Westervelt, D.M.; Horowitz, L.W.; Naik, V.; Tai, A.P.K.; Fiore, A.M.; Mauzerall, D.L. Quantifying PM_{2.5}-meteorology sensitivities in a global climate model. *Atmos. Environ.* **2016**, *142*, 43–56. [[CrossRef](#)]
28. Harrison, R.M.; Laxen, D.; Moorcroft, S.; Laxen, K. Processes affecting concentrations of fine particulate matter (PM_{2.5}) in the UK atmosphere. *Atmos. Environ.* **2012**, *46*, 115–124. [[CrossRef](#)]
29. Kassomenos, P.A.; Vardoulakis, S.; Chaloulakou, A.; Paschalidou, A.K.; Grivas, G.; Borge, R.; Lumberras, J. Study of PM₁₀ and PM_{2.5} levels in three European cities: Analysis of intra and inter urban variations. *Atmos. Environ.* **2014**, *87*, 153–163. [[CrossRef](#)]
30. Munir, S.; Habeebullah, T.M.; Mohammed, A.M.; Morsy, E.A.; Rehan, M.; Ali, K. Analysing PM_{2.5} and its association with PM₁₀ and meteorology in the arid climate of Makkah, Saudi Arabia. *Aerosol Air Qual. Res.* **2017**, *17*, 453–464. [[CrossRef](#)]

31. Wang, X.; Dickinson, R.E.; Su, L.; Zhou, C.; Wang, K. PM_{2.5} pollution in China and how it has been exacerbated by terrain and meteorological conditions. *Bull. Am. Meteorol. Soc.* **2018**, *99*, 105–119. [[CrossRef](#)]
32. Chen, Y.; Schleicher, N.; Fricker, M.; Cen, K.; Liu, X.-L.; Kaminski, U.; Yu, Y.; Wu, X.-F.; Norra, S. Long-term variation of black carbon and PM_{2.5} in Beijing, China with respect to meteorological conditions and governmental measures. *Environ. Pollut.* **2016**, *212*, 269–278. [[CrossRef](#)] [[PubMed](#)]
33. Yang, Q.; Yuan, Q.; Li, T.; Shen, H.; Zhang, L. The relationships between PM_{2.5} and meteorological factors in China: Seasonal and regional variations. *Int. J. Environ. Res. Public Health* **2017**, *14*, 1510.
34. Lin, Y.; Zou, J.; Yang, W.; Li, C.Q. A review of recent advances in research on PM_{2.5} in China. *Int. J. Environ. Res. Public Health* **2018**, *15*, 438. [[CrossRef](#)] [[PubMed](#)]
35. Li, L.; Qian, J.; Ou, C.Q.; Zhou, Y.X.; Guo, C.; Guo, Y. Spatial and temporal analysis of Air Pollution Index and its timescale-dependent relationship with meteorological factors in Guangzhou, China, 2001–2011. *Environ. Pollut.* **2014**, *190*, 75–81. [[CrossRef](#)] [[PubMed](#)]
36. Zhang, T.; Zhu, Z.; Gong, W.; Zhu, Z.; Sun, K.; Wang, L.; Xu, K. Estimation of ultrahigh resolution PM_{2.5} concentrations in urban areas using 160 m Gaofen-1 AOD retrievals. *Remote Sens. Environ.* **2018**, *216*, 91–104. [[CrossRef](#)]
37. Buchard, V.; da Silva, A.M.; Randles, C.A.; Colarco, P.; Ferrare, R.; Hair, J.; Winker, D. Evaluation of the surface PM_{2.5} in Version 1 of the NASA MERRA Aerosol Reanalysis over the United States. *Atmos. Environ.* **2016**, *125*, 100–111. [[CrossRef](#)]
38. Randles, C.A.; Da Silva, A.M.; Buchard, V.; Colarco, P.R.; Darmenov, A.; Govindaraju, R.; Shinozuka, Y. The MERRA-2 aerosol reanalysis, 1980 onward. Part I: System description and data assimilation evaluation. *J. Climate* **2017**, *30*, 6823–6850. [[CrossRef](#)] [[PubMed](#)]
39. Buchard, V.; Randles, C.A.; da Silva, A.M.; Darmenov, A.; Colarco, P.R.; Govindaraju, R.; Yu, H. The MERRA-2 aerosol reanalysis, 1980 onward. Part II: Evaluation and case studies. *J. Climate* **2017**, *30*, 6851–6872. [[CrossRef](#)]
40. Song, Z.; Fu, D.; Zhang, X.; Wu, Y.; Xia, X.; He, J.; Che, H. Diurnal and seasonal variability of PM_{2.5} and AOD in North China plain: Comparison of MERRA-2 products and ground measurements. *Atmos. Environ.* **2018**, *191*, 70–78. [[CrossRef](#)]
41. Van Donkelaar, A.; Martin, R.V.; Spurr, R.J.D.; Drury, E.; Remer, L.A.; Levy, R.C.; Wang, J. Optimal estimation for global ground-level fine particulate matter concentrations. *J. Geophys. Res. Atmos.* **2013**, *118*, 5621–5636. [[CrossRef](#)]
42. Van Donkelaar, A.; Martin, R.V.; Brauer, M.; Kahn, R.; Levy, R.; Verduzco, C.; Villeneuve, P.J. Global estimates of ambient fine particulate matter concentrations from satellite-based aerosol optical depth: development and application. *Environ. Health Perspect.* **2010**, *118*, 847–855. [[CrossRef](#)] [[PubMed](#)]
43. Huang, J.; Kondragunta, S.; Laszlo, I.; Liu, H.; Remer, L.A.; Zhang, H.; Petrenko, M. Validation and expected error estimation of Suomi-NPP VIIRS aerosol optical thickness and Ångström exponent with AERONET. *J. Geophys. Res. Atmos.* **2016**, *121*, 7139–7160. [[CrossRef](#)]
44. Peng, S.-S.; Piao, S.; Zeng, Z.; Ciais, P.; Zhou, L.; Li, L.Z.; Zeng, H. Afforestation in China cools local land surface temperature. *Proc. Natl. Acad. Sci. USA* **2014**, *121*, 2915–2919. [[CrossRef](#)] [[PubMed](#)]
45. Dawson, J.P.; Adams, P.J.; Pandis, S.N. Sensitivity of PM_{2.5} to climate in the Eastern US: a modeling case study. *Atmos. Chem. Phys.* **2007**, *7*, 4295–4309. [[CrossRef](#)]
46. Zhou, H.; Luo, Z.; Zhou, Z.; Li, Q.; Zhong, B.; Lu, B.; Hsu, H. Impact of different kinematic empirical parameters processing strategies on temporal gravity field model determination. *J. Geophys. Res. Solid Earth* **2018**. [[CrossRef](#)]
47. Zhou, H.; Luo, Z.; Tangdamrongsub, N.; Zhou, Z.; He, L.; Xu, C.; Li, Q.; Wu, Y. Identifying Flood Events over the Poyang Lake Basin Using Multiple Satellite Remote Sensing Observations, Hydrological Models and In Situ Data. *Remote Sens.* **2018**, *10*, 713. [[CrossRef](#)]
48. Zhou, H.; Luo, Z.; Tangdamrongsub, N.; Wang, L.; He, L.; Xu, C.; Li, Q. Characterizing drought and flood events over the Yangtze River Basin using the HUST-Grace2016 solution and ancillary data. *Remote Sens.* **2017**, *9*, 1100. [[CrossRef](#)]

